The Uncoupling of the Effects of Formins on the Local and Global Dynamics of Actin Filaments

Tünde Kupi,[†] Pál Gróf,[‡] Miklós Nyitrai,[†] and József Belágyi[†*]
[†]Department of Biophysics, Faculty of Medicine, University of Pécs, Pécs, Hungary; and [‡]Department of Biophysics and Radiation Biology, Semmelweis University of Medicine, Budapest, Hungary

ABSTRACT In this study, experiments were carried out in the conventional and saturation-transfer electron paramagnetic resonance (EPR) time domains to explore the effect of mDia1-FH2 formin fragments on the dynamic and conformational properties of actin filaments. Conventional EPR measurements showed that addition of formin to actin filaments produced local conformational changes in the vicinity of Cys-374 by increasing the flexibility of the protein matrix in the environment of the label. The results indicated that it was the binding of formin to the barbed end that resulted in these conformational changes. The conventional EPR results obtained with actin labeled on the Lys-61 site showed that the binding of formins could only slightly affect the structure of the subdomain 2 of actin, reflecting the heterogeneity of the formin-induced conformational changes. Saturation transfer EPR measurements revealed that the binding of formins decreased the torsional flexibility of the actin filaments in the microsecond time range. We concluded that changes in the local and the global conformational fluctuations of the actin filaments are associated with the binding of formins to actin. The results on the two EPR time domains showed that the effects of formins on the substantially different types of motions were uncoupled.

INTRODUCTION

Actin in polymerized form can be found in all eukaryotic cells as an essential structural and contractile element. In cellular structures, actin has diverse functions involving the maintenance of cellular shape, cell division and cell locomotion, and muscle contraction (1–3). The actin filament is usually described as a two-start, right-handed helix (4). Several studies have proven that the bending motion and torsional flexibility of the polymerized actin was important in its diverse function. Previous studies have shown that actin is a molecule having backbone motility as well as domains of different side-chain mobility (5,6). After polymerization, the marked reduction of the probe mobility was originally interpreted as evidence for the direct interaction of the monomers and/or for the phenomena whereby the motion is somehow trapped between neighboring monomers.

The dynamics of the actin cytoskeleton, its rapid assembly and disassembly, which is essential for many cellular functions, is regulated in vivo by various actin-binding proteins (ABPs) (7). Recently, two kinds of nucleators came into the focus of interest, namely Arp2/3 complex and formins, which are able to accelerate the actin assembly from pools of actin monomers. It is of interest which kind of conformational changes facilitate the interaction between actin and formin during and after the filament formation. Detailed investigations lead to the result that F-actin has a primary target for ABPs (8–10). The common binding motif, a hydrophobic cleft is formed between actin subdomain 1 and 3. The hydrophobic cleft is able to accommodate interactions with different ABPs. In subdomain 1, the Cys-374 residue is a suitable site for attaching reporter molecules. One of the numerous probes is the maleimide spin label (MSL), which can be attached without significant distortion of the structure. The MSL attached to Cys-374 residue of actin is in an excellent position to monitor interactions and conformational changes within the filaments. Its rotational correlation time can be measured in wide time range from 10^{-9} s to 10^{-3} s, which allows the detection of local and global conformational changes.

Previous fluorescence spectroscopic results showed that the binding of formins to the barbed end of the actin filaments made the actin filaments more flexible (11). In these studies, the effects of formins depended on the formin/actin concentration ratios, which were interpreted considering the end-binding and side-binding abilities of formin. At higher formin/actin, the formin saturated the binding sites at the side of the actin filaments and acted as molecular clamps. The effect was the stiffening of the filaments. The biological role and importance of the effects of formins on the actin filaments is unclear and needs further investigations. A possible approach to this direction is to describe the formin-induced conformational changes in more detail and to correlate them to the functions and interactions of actin and formin.

This study applies electron paramagnetic resonance (EPR) methods to better understand the formin-induced alterations in the actin filaments. The results provided direct evidence that local and global conformational fluctuations of the actin filament are associated with the interaction of formins with actin. Formin binding to the actin filaments resulted in the increase of the mobility of the probes on the nanosecond timescale, indicating that the microenvironment of the labels became more flexible. These data corroborate the previous results from fluorescence anisotropy experiments (11). On the other hand, the formins evoked a decrease of the mobility

Submitted June 2, 2008, and accepted for publication November 11, 2008.

*Correspondence: jozsef.belagyi@aok.pte.hu

Editor: David D. Thomas.

0006-3495/09/04/2901/11 $2.00

doi: 10.1016/j.bpj.2008.11.058

in the saturation transfer EPR time domain, which is characteristic for the torsional and/or bending motion of the filaments. These observations showed that the effects of formins on these two different types of motions were uncoupled and appeared to be independent of each other.

MATERIALS AND METHODS

Protein preparations

The FH2 domain of mammalian formin mDia1 was prepared as described previously (12). The protein fragments were expressed in *Escherichia coli* BL21 strain. Protein expression was induced with isopropyl-β-D-thiogalactopyranoside. Further purification of mDia1-FH2 fragments was carried out with size-exclusion chromatography using Sephacryl S-300. The protein concentration was determined spectrophotometrically at 280 nm with the extinction coefficient of 20,580 M^{-1} cm^{-1}. The purified formin fragments were stored at (80°C in storing buffer (50 mM Tris-HCl, pH 7.3 50 mM NaCl, 5 mM DTT, 5% glycerol).

Rabbit skeletal muscle actin was isolated from the aceton-dried powder from domestic white rabbit back muscles (13,14). The actin was stored in 4 mM Tris-HCl, pH 8.0, 0.2 mM ATP, 0.1 mM $CaCl_2$ (buffer A). The concentration of G-actin was determined photometrically at 290 nm with the absorption coefficient of 0.63 mg^{-1} ml cm^{-1} using a Shimadzu UV-2100 spectrophotometer. F-actin was prepared by the addition of 2 mM $MgCl_2$ and 100 mM KCl to buffer A.

Spin labeling of actin

Maleimido-TEMPO. Actin was labeled in F-form with *N*-(1-oxyl-2,2,6,6-tetramethyl-4-piperidinyl)-MSL in a molar ratio of 1:1.2 for 12 h at 2°C. Unreacted labels were removed by pelleting the actin by ultracentifugation. The pellet was resuspended, homogenized, and dialyzed in G buffer (4 mM Tris/HCl, pH 7.6, 0.2 mM ATP, 0.2 mM $CaCl_2$).

F-proxyl. G-actin was reacted with 1.2-fold molar excess of 3-(5-fluoro-2,dinitroanilino)-(1-oxyl-2,2,5,5-tetramethyl-3-pyrrolidine) (SL-FDNA) for 24 h at 2°C. The labeled G-actin was dialyzed against G buffer and used as SL-FDNA-G-actin or polymerized in F buffer (4 mM Tris/HCl, pH 7.6, 0.2 mM ATP, 2 mM $MgCl_2$). The concentration of actin in the EPR experiments was in the range of 50–100 μM. The labeled protein concentration was determined by comparison of the double integrals of spectra with known concentration of MSL-solution.

EPR measurements

Conventional and saturation transfer EPR spectra were taken with an ESP 300E (Bruker Biospin, Germany) spectrometer. First, harmonic in-phase absorption spectra were obtained by using 20 mW microwave power and 100 kHz field modulation with amplitude of 0.1 or 0.2 mT. Second, harmonic, 90° out-of-phase absorption spectra were recorded with 63 mW and 50 kHz field modulation of 0.5 mT amplitude detecting the signals at 100 kHz out of phase. The 63 mW microwave power corresponds in average microwave field amplitude of 0.025 mT in the center region of the cell, and the values were obtained by using the standard protocol of Squier and Thomas (15) and Fajer and Marsh (16). Spectra were normalized to the same number of unpaired electrons by calculating the double integral of the derived spectra. The concentration of bound labels was estimated by comparing the spectrum with maleimide spin label solution of known concentration. The spectra were stored in digitalized form and computer software, either WIN EPR programs from Bruker Biospin (Rheinstetten, Germany) or the ones developed in laboratory, were used to evaluate the spectral data. The programs allowed the subtraction of composed spectra into components and the determination of their fractions. It was also possible to estimate the distance between the low-field and high-field extreme after fitting of polynoms around these regions.

The protein samples were placed in two capillary tubes (Mettler ME-18552 melting point tubes); each of them contained 15 μl solution. The sample tubes were positioned parallel in the center region of the TM 110 cylindrical cavity. A small thermocouple was inserted in one of the capillary tubes, and the temperature was regulated with a diTC2007 type temperature controller. The spectra were usually recorded at 23 $\pm$ 0.1°C. Studying the EPR spectra of F-actin and F-actin samples in complex with formin as a function of temperature, the temperature was varied between 0°C and 60°C with an accuracy of 0.1°C.

Analysis of the slow-motional EPR spectra by computer simulation

To simulate the EPR spectra in the slow-motional region, the nonlinear least-squares (NLSL) program from Freed et al. (17,18) has been used. A graphical user interface for the Windows 32-bit operating system and some modifications of the source codes necessary for the Intel FORTRAN 9.1 compiler has been developed to the 1.51b version of the NLSL software and used earlier to simulate partially oriented slow-motional spectra for lipid systems (19). Among others, the NLSL software allows simulation of EPR spectra: 1), for Brownian rotational diffusion with anisotropic diffusion tensor; 2), taking into account tilt angle between the *g*-factor and the rotational diffusion tensors; and 3), with maximally three different components due to molecular environments or motion. Approximate values for the hyperfine splitting constants and *g*-factors of the spin label SL-FDNA has been first determined by measuring the isotropic hyperfine splitting, a_o found to be 1.589 mT, and calibrating the EPR spectrum measured at 60°C (g_o = 2.00553) against 2,2-diphenyl-1-picrylhydrazyl. In a series of preliminary simulations for the whole temperature interval best fits of EPR spectra resulted in the hyperfine- and *g*-tensors used further on in simulations: component 1: A_{xx}, A_{yy}, A_{zz} as 0.59, 0.60, and 3.48 mT, respectively; component 2: A_{xx}, A_{yy}, A_{zz} as 0.63, 0.63, and 3.43 mT, respectively; *g*-tensor: 2.00820, 2.00608, and 2.00230 for the slow-motional components and the mobile one. Tilt angles between the *g*- and diffusion tensors found to be different for the two slow-motional components and depend on the temperature.

RESULTS

In this study, the actin was labeled with spin probes (maleimido-TEMPO or F-proxyl), and either conventional or saturation transfer EPR measurements were carried out to characterize the dynamic and conformational properties of the actin before and after their interaction with formins (mDia1-FH2 domains).

Rotational motions in actin observed by spin labels

It is known from earlier experiments that Cys-374 incorporated more than 70% of the spin labels (MSL) under conditions used in our experiments, evidencing that the labeling procedure was selective (20–22). Conventional and saturation transfer EPR measurements reported that the labels on Cys-374 site were rigidly attached to the actin and reflected the motion of a larger domain in the monomer. According to our measurements with the actin filaments at room temperature, the hyperfine splitting constant $2A'_{zz}$ was 6.803 $\pm$ 0.010 mT (n = 22). The value of this parameter depends on the nanosecond rotational motion of the domain to which the spin label is attached. The diagnostic ST-EPR parameters L''/L and C'/C were estimated to be ~0.91 $\pm$ 0.05 (n = 12)

and 0.09 ± 0.12 ($n = 12$), respectively. The L''/L value corresponds to an effective rotational correlation time of ~100–120 μs. We similarly interpret these values assuming that the motion of the labels in F-actin reflected the torsional motion of several associated subunits (22,23).

It was shown in an earlier study using the reductive methylation method that in the monomer form of actin, the Lys-61 and Lys-113 are the most reactive residues (24). Upon polymerization their reactivity reduced significantly. Waring and Cook (25) reported that the spin label SL-FDNA could react with Lys-61 residue on G-actin. Fig. 1 shows the conventional EPR spectra of SL-FDNA-G-actin, SL-FDNA-F-actin, and MSL-F-actin at 22°C. The hyperfine splitting constant for the attached SL-FDNA label on F-actin was significantly smaller ($2A'_{zz} = 6.121 \pm 0.021$ mT, $n = 21$) than the hyperfine splitting for MSL-F-actin, which agrees with the previous observations that the environment of Lys-61 residue of the 9 kDa subdomain 2 has a smaller immobilizing effect on the probe molecule than that of the Cys-374 (25). The broad high-field hyperfine extreme in F-form of SL-FDNA-actin suggests that the spin label attached to the Lys-61 residue has either two conformations possessing different rotational dynamics or one fraction of the labels located on a different site, for example on Lys-113 residue. In contrast, in the G-form of SL-FDNA-actin, only one hyperfine splitting value could be derived, suggesting that the probe likely attached to only one location in the monomer. In this case the mean value of the $2A'_{zz}$ was equal to 5.912 ± 0.05 mT ($n = 7$).

To confirm the binding of SL-FDNA to Lys-61, G-actin was labeled with fluorescence isothiocyanate. Reaction of G-actin with fluorescein isothiocyanate (FITC) resulted in the attachment of the probe to Lys-61 of the 9 kDa subdomain 2 of the actin. The FITC-labeled G-actin was unable to polymerize in the absence of phalloidin in accordance with previous observations (26). After exhaustive dialysis in G buffer, we attempted to label the FITC-G-actin with SL-FDNA. After incubation with SL-FDNA the sample showed an EPR spectrum with a large fraction of labels attached to weakly immobilizing sites. The total actin-bound spin concentration of the double-labeled sample reduced to ~20% of that achieved in the absence of FITC, its $2A'_{zz}$ was smaller with ~1.5 G, and the ratio I_{+1}/I_m (9.25) was ~30 times higher than that of the SL-FDNA-actin. (See definition of parameter I_{+1}/I_m in Fig. 2.) This experimental result supports the former finding that the dominating part of the spectrum for SL-FDNA-actin is arising from labels on Lys-61.

Using the average rigid limit of the hyperfine splitting constant obtained from spectral simulation (6.915 mT), the apparent rotational correlation time for the motion of the SL-FDNA label on G-actin was estimated to be ~8–9 ns (27). This value is shorter than the rotational correlation time of the whole monomer molecule (~18 ns), indicating that the probe motion reflects the motion of a subdomain of the actin monomers. The results of EPR parameters are summarized in Tables 1 and 2.

Effect of formin on rotational mobility

In the first set of experiments, MSL-labeled F-actin was used. Different amounts of formin were added to spin-labeled F-actin. The molar ratios of actin/formin were 50:1, 25:1, 10:1, and 5:1. Binding of formin to the MSL-F-actin decreased the hyperfine splitting constant (Table 1). This effect was similar to that induced by the binding of myosin or heavy meromyosin to F-actin, which was explained by the increased shielding from solvent (20, 28). In the case of formins, this explanation seems to be unlikely, because formins bound preferably to the ends of the filaments due to tight formin affinities to the ends and to the low formin/actin. Analysis of spectra by the line width of the low-field

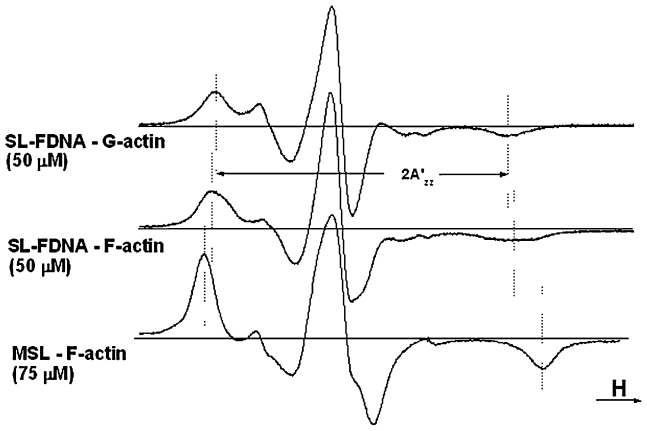

FIGURE 1 Conventional EPR spectra of MSL-F-actin, SL-FDNA-G-actin, and SL-FDNA-F-actin. SL-FDNA probe molecules in the environment of the Lys-61 residue reported larger mobility in comparison to MSL-F-actin samples. Deconvolution of SL-FDNA-F-actin spectrum resulted in two components. The concentration of actin samples were 75 μM (MSL-F-actin) and 50 μM (SL-FDNA-F-actin), respectively.

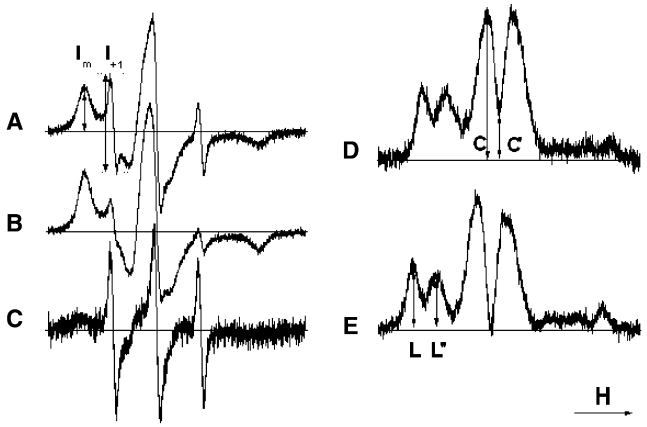

FIGURE 2 Conventional and saturation transfer EPR spectra of MSL-F-actin in interaction with formin. (*A*) F-actin + formin (25:1 M/M); (*B*) F-actin; (*C*) difference spectrum of *A* and *B*; (*D*) F-actin + Formin (25:1 M/M); (*E*) F-actin. Actin concentration was 50 μM to obtain conventional spectra and 100 μM to obtain ST-EPR spectra.

TABLE 1 Mobility changes in the C-terminal domain of actin after formin binding

	Actin/formin concentration (mol/mol)				
	No formin	50:1	25:1	10:1	5:1
Conventional EPR technique					
Number of parallels	22	14	15	13	3
$2A_{max}$ (mT)	6.803 ±0.008	6.764 ±0.011	6.758 ±0.009	6.749 ±0.011	6.737 ±0.030
Saturation transfer EPR technique					
Number of parallels	12	10	8	10	3
L''/L	0.916 ± 0.05	1.120 ± 0.06	1.038 ± 0.06	1.057 ± 0.06	1.179 ± 0.08
C'/C	0.12 ± 0.09	0.321 ± 0.08	0.339 ± 0.06	0.335 ± 0.06	0.276 ± 0.11
Intensity ratio of the two first peaks					
Number of parallels	8	6	5	5	2
I_{+1}/I_m	0.89 ± 0.06	1.68 ± 0.16	1.82 ± 0.21	2.06 ± 0.17	1.61 ± 0.5

Probe molecules on Cys-374. Maleimide nitroxide spin labels were covalently attached to Cys-374 site of F-actin. Double integrals of the EPR spectra showed that ~70% of actin monomers were labeled. Different amount of formin was added to F-actin and the samples were stored at 4°C for 16 h before EPR measurements. Data presentation: mean ± SE, at actin to formin 5:1 mol/mol: mean ± SD and difference of mean at I_{+1}/I_m.

line as suggested by Mason and Freed (29) showed that after binding of formin to F-actin, the rotational correlation time of the label in the environment of the Cys-374 sites decreased from ~50 ns to ~30 ns at 25:1 molar ratio of actin/formin. Similarly, decreased rotational correlation times were calculated at other actin/formin.

According to the EPR spectra, the addition of formins to actin filaments produced another conformational change in the actin protomers. One fraction of the bound spin labels appeared in a more mobile state after the binding of formin (Fig. 2). The mobilizing effect was more pronounced in the spectra at lower concentrations of actin (<40 μM).

The peak/peak of the first two peaks is defined as I_{+1}/I_m, whereby I_m is the amplitude of the low-field maximum and I_{+1} is the amplitude of the first spectral line in the newly generated spectrum reflecting the fast motion of the label (see Fig. 2). Values of this ratio as a function of the formin/actin molar are given in Table 1. It shows that formin binding produces a marked increase of I_{+1}/I_m, but the change does not exhibit a remarkable variation at increasing formin concentration, and above at 10:1 actin/formin concentration a decrease was already detected. Spectrum subtraction by computer showed that the double integral of the more mobile component of the spectrum did not exceed 10% of the total EPR absorption. To avoid the dilution of sample by addition of formin (which usually had a smaller concentration than actin), the same volume of buffer solution was added to the F-actin sample in control measurements. The possible effect of viscosity change was tested by the addition of the inert protein bovine serum albumin using the same molar ratio to actin as in the case of formin. No remarkable effect was experienced after the addition of the albumin in the line shape of EPR spectrum. Therefore, we can conclude that binding of formin to the actin filaments induced the mobilization of the segment containing the reporter molecule. The rotational correlation time of this faster motion was estimated to be 0.3 ns, which was not far from the rotational correlation time of the free label. The calculation is based on the formula by line/height published by Schreier et al. (30).

TABLE 2 EPR spectral parameters of spin-labeled F-actin and its complexes with formin

	F-actin/formin (mol/mol)				
	No formin	50:1	25:1	10:1	5:1
Conventional EPR technique					
Number of parallels	15	12	7	8	3
$2A_{max}$ (mT)*	6.121 ±0.021	6.070 ±0.011	6.071 ±0.019	6.055 ±0.016	6.037 ±0.030
Saturation transfer EPR technique					
Number of parallels	7	3	3	4	None
L''/L	0.415 ± 0.05	0.463 ± 0.13	0.638 ± 0.17	0.762 ± 0.40	Noisy spectra
C'/C	−1.172 ± 0.05	−1.088 ± 0.20	−1.056 ± 0.12	−0.838 ± 0.30	Noisy spectra

Probe molecules on Lys-61. Fluoro-dinitroanlino-proxyl nitroxide spin labels were covalently attached to Lys-61 site of G-actin. Double integrals of the EPR spectra showed that ~30–35% of actin monomers were labeled. Different amount of formin was added to actin after polymerization, and the samples were stored at 4°C for 16 h before EPR measurements. Data presentation: mean ± SE, F-actin + formin (5:1 mol/mol): mean ± SD.

*One-way ANOVA showed that variation among sample means was not significant ($p = 0.062$). The hyperfine splitting (hfs) values of F-actin and the complexes of F-actin and formin prepared from the same batch were compared with sign-test. The difference in molar ratios was not taken into account during comparison of pairs. To obtain the signs, we recorded ''plus'' whenever the hfs value of F-actin was lower, and ''minus'' when the hfs value of F-actin was larger than the corresponding value of the complex. The total number of minus was 22, and the number of plus was 7; in one case the difference was zero. The mean difference between pair of numbers was significant on the probability level of $p = 0.05$.

In saturation transfer EPR measurements, different effects of formin binding to F-actin were observed. This technique is sensitive to motions on a longer timescale than the conventional EPR spectra. Both diagnostic EPR parameters, L''/L and C'/C, reflected increased immobilization of labels after addition of formin to MSL-F-actin filaments (Fig. 2). However, only moderate changes were derived in the ST-EPR parameters at increasing molar ratio of formin/actin (Table 1). To have an indication about the change of rotational motion after binding of formin to F-actin, the nomograms published by Thomas et al. (31) for Brownian rotational diffusion were used. The estimated effective rotational correlation time increased from 100 to 120 μs to 150 μs (derived from low-field diagnostic parameter L''/L) and from 7 μs to 40 μs (using parameter C'/C) for the actin filaments after the binding of formins.

The conventional EPR spectra of MSL- and SL-FDNA-F-actin and their complexes with different amount of formin exhibited rotational motion in the nanosecond time domain as well. This nanosecond motion can affect the ST-EPR spectra. However, the use of integrated intensity parameters for evaluation of ST-EPR spectra is effective to minimize errors arising from weakly attached probe molecules. Following the method suggested by Squier and Thomas (15), we calculated the integrals of the ST-EPR spectra of pairs of F-actin and different F-actin-formin complexes from the same batch. The integrals of these spectra were divided by the double integrals of the corresponding conventional EPR spectra and by the microwave intensity in the cavity. The intensity parameters were normalized to the rigid limit value of F-actin (F-actin + 40% w/w sucrose at (18°C). The calculated values were 0.107 ± 0.012 SE ($n = 5$) for F-actin and 0.158 ± 0.029 SE ($n = 9$) for F-actin + formin. During this calculation process formin/actin was not taken into account. The increase of the intensity parameter is sign of the increased rotational correlation time. Therefore, this result is in agreement with calculation obtained with line/height parameters L''/L and C'/C, that is, the addition of formin to F-actin induced a decrease of the microsecond rotational motion of F-actin filaments.

After the addition of formin to SL-FDNA-labeled F-actin, the conventional EPR spectra showed small spectral changes, which could be characterized with increased mobility in the nanosecond time range (Fig. 3). Similarly to MSL-F-actin, this mobile fraction was almost independent of the formin/actin molar below 0.1, and the double integral of this fraction was always smaller than 5% of the total actin concentration. We detected differences between the hyperfine coupling constant of F-actin and that of F-actin in complex with formin as well. The mean values of the differences were not significant. However, when we used the nonparametric sign-test for evaluation of the differences of [$2A'_{zz}$ (F-actin + formin) − $2A'_{zz}$ (F-actin)], taking all experimental data together independent of actin/formin molar, the small decrease of the hyperfine splitting constant was already

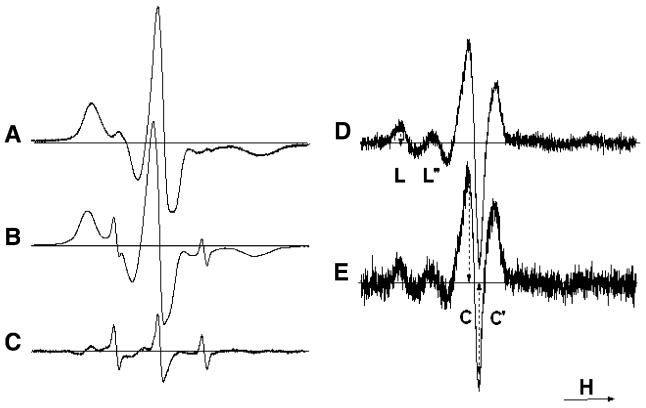

FIGURE 3 Conventional and saturation transfer EPR spectra of SL-FDNA-F-actin in interaction with formin. (*A*) F-actin; (*B*) F-actin + formin (25:1 M/M); (*C*) Difference spectrum of *A* and *B*; (*D*) F-actin; (*E*) F-actin + formin (25:1 M/M) F-actin. The actin concentration was 75 μM.

significant at the probability level of $p = 0.05$. It suggests that the conformational change induced by binding of formin to F-actin produced an increase in mobility in the environment of the paramagnetic label attached to the lysine residue in the subdomain 2. In contrast, ST-EPR measurements on SL-FDNA-F-actin and F-actin-formin at actin concentrations of 120–150 μM showed an increase of the diagnostic parameters L''/L and C'/C (Fig. 3).

Fig. 4 summarizes the relative change of the rotational motion in percent for MSL- and SL-FDNA-F-actin as a function of formin/actin molar. Nanosecond and microsecond rotational motions show weak relationships between rotational motion of labels and molar ratio of formin/actin. It is known from earlier data from literature that formin can bind to the barbed end of actin filaments and also alongside of filaments. It seems this basic property of formin is reflected in the above relationships; the decrease of the rotational correlation time on the nanosecond timescale is related to the local conformational change in subdomain 1, whereas the nonspecific binding of

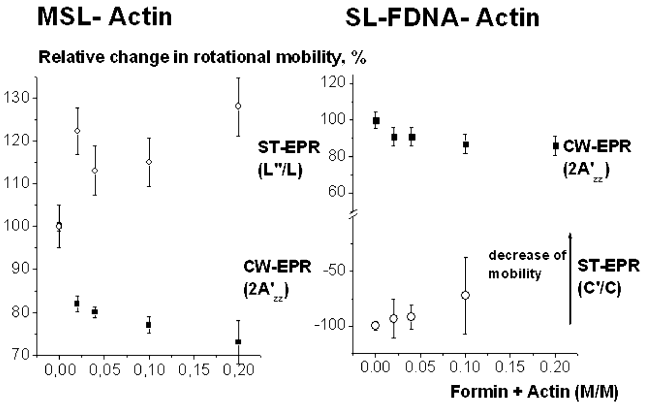

FIGURE 4 Relative changes of rotational mobility of spin labels in percent bound to MSL- and SL-FDNA-actin after addition of formin. Note: in the submicrosecond time domain the ST-EPR parameter C'/C has negative sign.

formin to the filaments is responsible for the decrease of torsional motion on microsecond timescale.

In a series of experiments, SL-FDNA-G-actin was reacted with different amounts of formin to see whether the labeling of G-actin at Lys-61 site might affect the formin-induced polymerizability of actin and the interaction of formin with the newly formed F-actin. The results are summarized in Table 3. Table 4After 16 h, storage EPR measurements were carried out and the spin concentrations of samples were determined. After EPR measurements the samples were centrifuged for 30 min at 380,000 × *g* and the supernatants were measured again. The calculated ratio of the spin concentration and the remaining G-actin in supernatant as a function of formin/actin is included in Table 3. By subtracting the spectrum of G-actin from the spectra of the actin-formin complexes, it was possible to estimate the value of the larger hyperfine splitting constant (Fig. 5). These experiments support the view that formin is able to induce the polymerization of SL-FDNA-G-actin, and the modification of actin by SL-FDNA might affect only marginally the formin-actin interaction.

Effects of the temperature on actin and its complexes with formin

We extended our studies to describe the formin-induced conformational changes in actin filaments at different temperatures. Fig. 6 *A* shows the temperature dependence of the $2A'_{zz}$ for F-actin and for the F-actin-formin complex (actin/formin was 25:1). In both cases (± formin), the dependence of the calculated $2A'_{zz}$ on the 1000/T was linear.

Although similar results were obtained at different actin/formin (data not shown), the calculated regression coefficients, designated by *b*, differed slightly for different actin/formin; at the molar ratio of 1:25 formin/actin, the *b* values were 0.392 ± 0.008 and 0.519 ± 0.014 for F-actin and F-actin/formin, respectively, whereas at 1:5 formin/actin *b* values of 0.402 ± 0.018 and 0.540 ± 0.022 were calculated for F-actin and F-actin/formin, respectively. The $2A'_{zz}$ values for the actin-formin complexes were smaller than that of F-actin in the whole investigated temperature range, and the regression coefficients of the fitted straight lines of F-actin and F-actin-formin complex were significantly different at the probability level of $p = 0.05$. However, it should be noted that the regression coefficients of the actin-formin complexes at different molar ratios were not significantly different from each other at the probability level of $p = 0.05$. These results show that 1), the binding of formin to actin caused a conformational transition in the environment of the C-terminal in the subdomain 1 of actin, in correlation with our observation made at 22°C; and 2), the formin-induced effects did not depend strongly on formin/actin. The latter conclusion is supported by the fact that at higher temperatures, close to the thermal denaturation temperature, an earlier decrease of $2A'_{zz}$ was detected in the case of actin-formin complex, indicating that the formin induced loosening of structure of the filaments resulted in a lower heat denaturation temperature of actin. This observation is in agreement with the calorimetric results published previously (11). Temperature-dependent experiments carried out on MSL-F-actin and MSL-F-actin-formin complexes gave linear dependences between the changes of hyperfine splitting constant and the reciprocal absolute temperature for all samples. To obtain an explanation for the linear dependence of the differences [$2A'_{zz}$ (0°C) − $2A'_{zz}$ (*t* °C)] against 1000/T, we assumed that $2A'_{zz}$ (0°C) was approximately equal to the rigid limit of the hyperfine splitting constant $2A_{zz}{}^{r}$. The rotational correlation time for the bound spin label can be calculated according to Goldman equation (27)

$$\tau_2 = a\left(1 - \left(2A'_{zz}/2A^{r}_{zz}\right)\right)^{b}, \quad (1)$$

where $a = 5.4 \times 10^{-10}$ s and $b = -1.36$. Starting with the logarithmic form of the equation

TABLE 3 EPR spectral parameters of spin-labeled G-actin and its complexes with formin

	Actin/formin (mol/mol)					
	No formin	50:1	25:1	10:1	5:1	F-actin
$2A'_{zz}$(mT)*	5.906 ± 0.006 (8)	5.981 ± 0.016 (7)	6.052 ± 0.015 (11)	6.059 ± 0.016 (9)	6.125 ± 0.012 (4)	6.083 ± 0.031 (9)
$2A'_{zz}$(mT)†	—	6.518 ±0.08 (5)	6.562 ± 0.042 (5)	6.548 ± 0.02 (4)	6.528 ± 0.06 (4)	6.504 ± 0.04 (4)
R‡	none	0.146	0.280	0.514	0.549	0.563
I_{+1}/I_m§	0.841	2.040	2.028	2.047	2.129	0.579
G-actin in supernatant (%)§	96	80	46	14	4	3

Fluoro-dinitroanilino-proxyl nitroxide spin labels were covalently attached to Lys-61 site of G-actin. Double integrals of the EPR spectra showed that ~30–35% of actin monomers were labeled. Formin was added in different molar ratio to globular actin and the samples were stored at 4°C for 16 h before EPR measurements. Data presentation: mean value ± SE, except F-actin + formin (5:1 mol/mol); mean ± SD.

*In polymerized form of SL-FDNA-actin and actin-formin complexes the EPR spectra were superposition of two spectra with different hyperfine splitting constants. The data (except G-actin) in Table 3 represent the average value of the smaller $2A'_{zz}$ values, which are only estimated values of the real hyperfine splitting constants. Numbers in parenthesis show the number of parallels.

†Hyperfine splitting constant of the difference spectrum. The EPR spectrum of G-actin was subtracted from the recorded spectrum to obtain the larger hyperfine splitting value.

‡*R*-value shows the ratio of F-actin-like component of the spectrum with respect to the total spin concentration of the sample. Mean values of two parallels.

§Mean values of three parallels.

TABLE 4 Spectral characteristics based on model of EPR simulations

T (°C)		Components	
		I	II
0			
	%	63.6	36.4
	τ_{prp}(ns)	3941*	136
	τ_{pll}(ns)	5	2
	τ_{ave}(ns)	146.3	14.7
	α_D	84	28
	β_D	7	35
30			
	%	48.4	51.6
	τ_{prp}(ns)	165	28
	τ_{pll}(ns)	0.1	0.1
	τ_{ave}(ns)	4.7	1.9
	α_D	88	2
	β_D	16	28
60			
	%	28.3	71.7
	τ_{prp}(ns)	204	45
	τ_{pll}(ns)	0.1	0.1
	τ_{ave}(ns)	5.2	2.5
	α_D	59	1
	β_D	21	30

I and II represents the slower and faster slow-motional components. τ_{prp} and τ_{pll} characterize the perpendicular and parallel rotational correlation time of the diffusion tensor. τ_{ave} denotes an apparent correlation time used to calculate as the square root of the product of τ_{prp} and τ_{pll}. α_D and β_D are the spherical tilt angles between the g-factor and the diffusion tensors. Residual amplitudes normalized to the experimental spectra were calculated as the normalized deviation between simulated and experimental spectra. Averages and standard deviations of these normalized residual amplitudes were found to be better than $0.9 \pm 0.72\%$.

*This value is an overestimate of the rotational correlation time, because the sensitive range for the correlation time of the NLSL programs is smaller than 1 μs.

$$\ln \tau_2 = \ln a + b \ln\left(1 - \left(22A'_{zz}/2A^r_{zz}\right)\right) \quad (2)$$

from that one can obtain that $\ln\tau_2$ is proportional to the difference of the hyperfine coupling constant, and the latter is proportional to the reciprocal of the absolute temperature

$$\ln \tau_2 = \left(b/2A^r_{zz}\right)\left(2A^r_{zz} - 2A'_{zz}\right) + (\ln a - b) \propto 1000/\mathrm{T}. \quad (3)$$

The decrease of ln τ_2 indicates an Arrhenius-type relationship, the change of hyperfine splitting constant is solely due to the increase of temperature. From the linear plots of ln τ_2 against 1000/T, the activation energies were calculated; they were $E_a = 18$ kJ/mol for F-actin and $E_a = 15$ kJ/mol for F-actin-formin complex. As rigid limit $2A_{zz} = 7.055$ mT was used. This value of the rigid limit was obtained on an MSL-F-actin sample with 40% sucrose by weight at -18°C.

Different character in temperature dependence of actin and actin-formin complex was obtained when the FDNA-label was attached to Lys-61 residue (Fig. 6 *B*). Instead of linear dependence between $2A'_{zz}$ and 1000/T, we observed a sigmoidal shape for actin and actin-formin complex as well. Moreover, no difference could be established between actin and actin-formin complex.

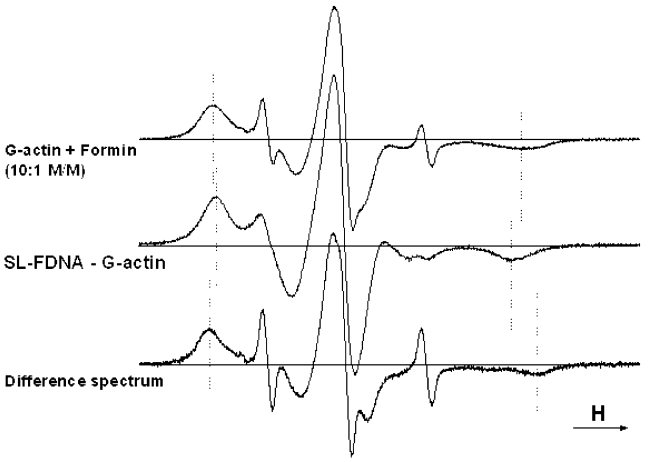

FIGURE 5 Addition of formin to SL-FDNA-G-actin increased the mobility of one fraction of probe molecules in the environment of Lys-61 site and at the same time the high-field component, which is characteristic on SL-FDNA-F-actin-formin complex also appeared (*upper spectrum*). Bottom: difference spectrum was obtained after subtraction of the spectrum of SL-FDNA-G-actin (*middle spectrum*) from the recorded spectrum.

The EPR measurements on SL-FDNA-F-actin correlate with earlier biochemical results. According to our experiments, the amount of labeled monomers varied between 30% and 40% of the total monomer concentration in agreement with former findings (25). On the other hand, the broad high-field extreme referred to the presence of two superimposed spectra (Fig. 1). The temperature dependence of EPR spectra suggests that 1), either the paramagnetic molecules attached to Lys-61 have two conformations indicating that the protein environment has also two conformations around the Lys-61 residue, and the relative

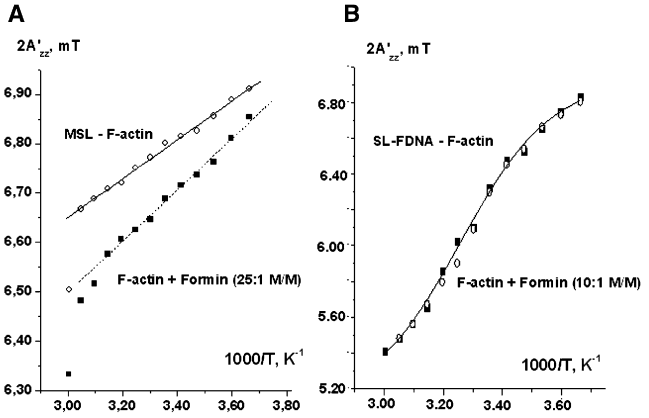

FIGURE 6 Changes of hyperfine splitting constants of spin-labeled F-actin as a function of temperature. (*A*) MSL-F-actin (○) and MSL-F-actin (■) in complex with formin (25:1 M/M). (*B*) SL-FDNA-F-actin (○) and its complex with formin (10:1) (■). The heat absorption produced an earlier denaturation of MSL-F-actin + formin complex at ~55°C. The concentration of spin-labeled actin was 100 μM in both cases.

contributions of the two conformations depend on temperature; or 2), one fraction of the labels are located on Lys-61 site and the other fraction is attached to other site, e.g., Lys-113. The temperature dependence of the contribution of the two components suggests that the former explanation is more likely.

A careful inspection of two spectra, measured at 0°C and 60°C, showed that although there are two components present in both cases, it is only one of them that determines the hyperfine coupling constants, which can be measured in these cases. This suggestion was confirmed by spectrum simulation presented below. Thus we attempted to fit the outer extrema as the function of temperature by a sigmoidal Boltzmann-function:

$$2A'_{zz}(z) = \left[\left(2A'_{zz,\min} - 2A'_{zz,\max}\right)/\left(1 + \exp(z - z_0/\delta z)\right)\right] + 2A'_{zz,\max}, \quad (4)$$

where z_0 is the point of inflection and δz is the rate of growth. The best fit was found with the parameters $z = 1000/\mathrm{T}$; $z_0 = 3.256$ (34°C); $\delta z = 0.155$ with $2A'_{zz,\min}$ and $2A'_{zz,\max}$ equal to 5.10 and 6.94 mT, respectively. $2A'_{zz,\min}$ and $2A'_{zz,\max}$ is the smallest and largest hyperfine splitting obtained during the measurements. The sigmoidal relationships for actin and actin-formin complexes were almost exactly the same evidencing that binding of formin did not produce large significant mobility change in subdomain 2 and did not affect remarkably the populations of the two conformations. The observed asymmetric shapes of the low-field signals (see on the EPR spectrum measured at 0°C Fig. 7, curve *A*) and especially of the broadened high-field signals around 30°C (Fig. 7, *curve B*) suggested that at least two populations have to be taken into account to analyze the temperature-dependent $2A'_{zz}$ values. A spectral subtraction revealed also that the EPR spectra (e.g., at 0°C) contain a signal arising from a subpopulation of actin molecules undergoing slow motion, at least around one axis of rotation (Fig. 7, *curve A-B*). A partial subtraction of the spectrum obtained at 30°C from that at 60°C gave the other portion of the actin molecules, which possesses the shortest rotational correlation time (Fig. 7, *curve C-B*). These spectral subtractions resulted in spectra with almost symmetric low-field and high-field extremities, which can be characterized by one correlation time.

Spectral simulations of the EPR spectra measured at different temperatures showed that none of the spectra can be described by a single slow-motional component (the presence of a mobile component can be seen on all of the experimental spectra, but it is negligible below ~30°C). We also found that an isotropic Brownian rotational diffusion cannot describe the rotation of the Lys-61-labeled F-actin. To minimize the parameters used in our spectral simulations, we used axial symmetry for the diffusion tensor that can be characterized by the corresponding τ_{prp} and τ_{pll}, perpendicular and parallel rotational correlation times,

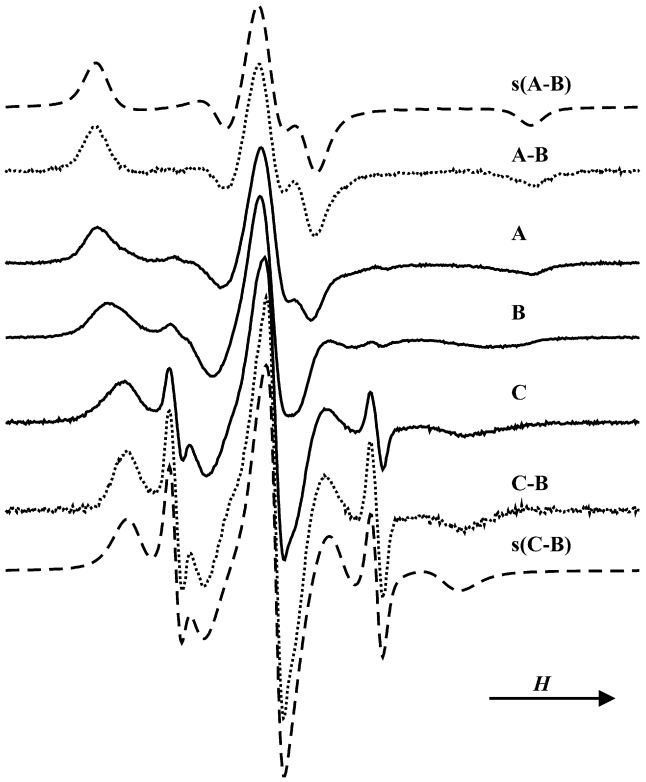

FIGURE 7 EPR spectra of Lys-61 labeled actin. *A*, *B*, and *C* experimental spectra measured at 0°C, 30°C, and 60°C, respectively. (*A* and *B*) difference spectrum of *A* and *B* (with appropriate subtraction coefficient); (*C* and *B*) difference spectrum of *C* and *B* (with appropriate subtraction coefficient); *s*(*A-B*) and *s*(*C-B*): best fit simulated spectra of *A-B* and *C-B*, respectively.

respectively. Our spectral simulation showed that coincident g- and diffusion tensors cannot correctly fit the experimental spectra; and the two slow-motional components possess different spherical tilt angles (α, β) between the tensors, having greater α-values for the slower and smaller ones for the faster components. The differences found in α-tilt angles are significant, because using the same values for both components did not result in satisfying fits of the experimental spectra. On the contrary, β-values for the faster component can be taken as identical, because we found only a small improvement in the chi-quadrate values, which characterizes the goodness of fit (Table 4). In Fig. 8, there are three representative experimental and simulated spectra showing the contributions due to the slow-motional components, and also the mobile ones at 30°C and 60°C, having a proportion of ~1 and 6%, respectively.

DISCUSSION

In this study, we described the formin-induced conformational changes in actin filaments by using EPR methods. The application of the EPR spectroscopy has advantages against other spectroscopic techniques applied earlier: 1), it was possible to label the monomer actin at Lys-61 site

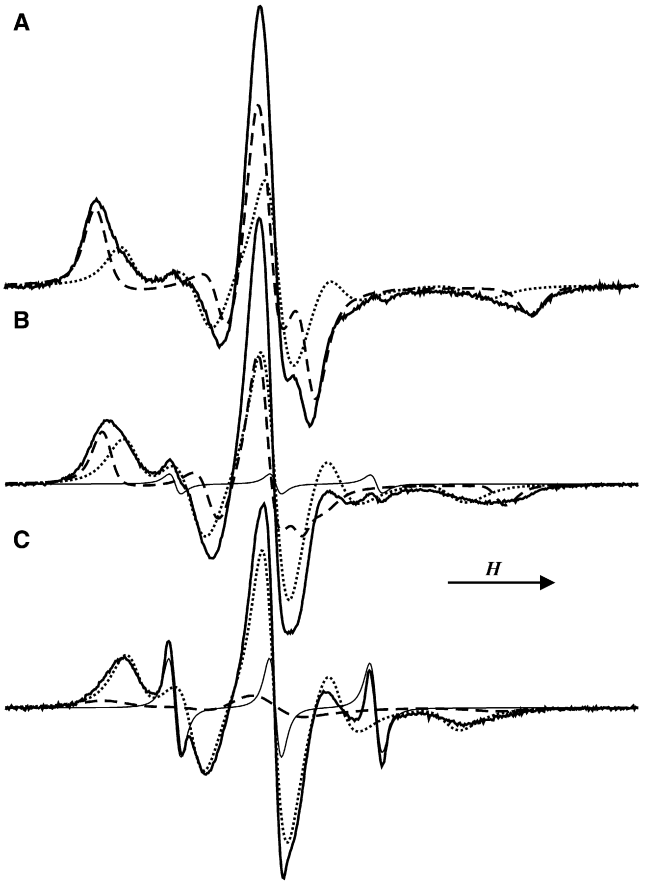

FIGURE 8 EPR spectra of Lys-61 labeled actin. Solid lines: experimental spectra; dashed lines: contribution due to slower components; dotted lines: contributions due to faster components; narrow lines: mobile components. Spectra, denoted as *A*, *B*, and *C* correspond to signals obtained at 0°C, 30°C, and 60°C, respectively.

with paramagnetic reporter molecules and to study the formin-induced effects in different locations of the actin protomers (C-terminal and subdomain 2); 2), it was also possible to identify the two different conformations of SL-FDNA-F-actin by spectral simulation and to derive their changes at different temperatures; and 3), different EPR techniques (conventional and saturation transfer) allowed the study of local and global conformational changes after binding of formin to actin.

Addition of formin to F-actin resulted in two main observations in the conventional EPR spectra (Figs. 2 and 6): 1), formin induced a local mobility increase in the environment of the labeled sites, the mobility of the affected sites can be characterized with a rotational correlation time that is not far from the rotational motion of the free labels; and 2), according to the analysis by the lifetime broadening method the addition of formin induced a mobility increase in the time range of 10 ns in environment of the labeled sites of F-actin, and changes depended slightly on the molar ratio of formin/actin.

The evaluation of the conventional EPR spectral parameters showed that after the addition of formin to MSL-F-actin or to SL-FDNA-F-actin, the hyperfine splitting constant characterizing the actin filaments decreased (Figs. 2 and 6).

The formin effect was more pronounced in the case of MSL-F-actin. This can be explained by accepting that spin labels attached to Lys-61 residues reflect, to higher extent, the local mobility of the domain to which they attach, whereas MSL is localized in a more rigid environment. Thus if there is a change in the internal mobility of the actin protomers, this can evoke a higher relative change in a more rigid environment than in a more mobile one. Based on the EPR data, we cannot exclude that the change of hyperfine splitting constant was due to the change of polarity in the environment of the label after binding of formin to actin. However, this possibility appears to be unlikely because these experiments were carried out at low formin/actin concentration ratios. The effect of formin saturated at ~1:10. Under these already-saturating conditions only a small fraction of EPR probes could establish direct interactions with the formins. On the other hand, independent evaluation method of spectra based on the variation of the line width at different formin/actin resulted in decreasing rotational correlation time with increasing formin concentration in the conventional EPR time domain. Therefore, we concluded from these observations that the binding of formins to actin increased the mobility of the probes, indicating that the protein matrix in the local environment of the spin labels became more flexible. The importance of the correlation is underlined by the fact that both the conventional EPR and fluorescence methods reported changes on the nanosecond timescale.

The observation that the effect of formin reached its maximum at low formin/actin concentration ratios drives to another conclusion. The mDia1-FH2 can bind to the sides of the actin filaments in a 1:1 stoichiometry and the affinity of this binding is weak (~3 μM (11)). Considering the low formin/actin concentration ratios applied here and the formin concentration dependence of the effect, we excluded that the observed formin effects were due to the binding of the mDia1-FH2 to the sides of the filaments. On the other hand, the affinity of mDia1-FH2 for the barbed end of actin is tight (20–50 nm (33,34)), and the concentration of the barbed ends was a few nm in these experiments providing appropriate conditions for the saturation of these binding sites. We concluded, therefore, that formin modified the conformation of the actin filaments by binding to their barbed end.

We calculated from the EPR spectra that the concentration of actin exhibiting shorter rotational correlation time was 4–5% of the total actin concentration, but not more than 10%. Assuming that the labeled protomers have a uniform distribution along the actin filaments and ~2000 protomers form an actin filament (length of filaments: 4.2–5 μm (23)), 4–5 percent modified actin would mean that the conformation 80–100 protomers was altered by the formin binding to the

barbed end in each filaments. This result shows that the effect of binding of formin to the barbed end extended over longer distances alongside the filaments suggesting the presence of long-range allosteric interactions.

In contrast to the results from the conventional EPR experiments, the saturation transfer spectral parameters reported increased immobilization with increasing molar ratio of formin/F-actin, indicating that the torsional flexibility of the actin filaments decreased. Temperature-dependent measurements of the hyperfine splitting constant of MSL-F-actin in the interval from 0°C to 65°C showed linear dependence as a function of reciprocal absolute temperature for F-actin and F-actin-formin complex. Corroborating our results at 22°C, the hyperfine splitting constant $2A'_{zz}$ were smaller at all temperatures for the F-actin-formin complexes than for the F-actin in the absence of formin. The regression coefficients of the fitted straight lines of F-actin and F-actin-formin complex were significantly different at the probability level of $p = 0.05$, indicating that the binding of formin to actin caused a conformational transition in the environment of the C-terminal in the subdomain 1 of actin. Previous measurements reported that the denaturation temperature for F-actin was affected by ABPs (35, 36). It was observed that formins decreased the denaturation temperature of the actin filaments (11). In our EPR experiments, the actin-formin complex had a larger slope, had smaller activation energy, and exhibited an abrupt change at temperatures lower than for the F-actin. These observations are the signs of a lower denaturation temperature, in agreement with the results of calorimetric experiments (11).

Previous fluorescence spectroscopic experiments showed that formin binding to the barbed end of actin filaments made the filaments more flexible (11, 32). These methods were predominantly sensitive to motions on the nanosecond and submicrosecond timescale. In the study presented here, this timescale was also involved in the investigations carried out by the conventional EPR methods. The results corroborated the earlier conclusions regarding the effects of formins on the conformation of actin filaments. Further to these observations, these results extended the description of the formin-induced intramolecular changes to those apparent on longer timescales (microseconds), i.e., to the torsional and/or bending motions of the filaments. The data indicated that the torsional flexibility of the filaments decreased upon formin binding. The opposite direction of the changes observed on these two different timescales suggests that the formin-induced conformational changes are complex in the actin filaments.

CONCLUSIONS

EPR experiments obtained here on the interaction between spin-labeled actin and actin-formin complexes resulted in two main observations. The addition of formin to actin filaments produced a local mobility increase in the microenvironment of the Cys-374 in the conventional EPR time domain. The effect of formin on the label attached to the Lys-61 was little indicating that the distribution of the formin-induced conformational changes was heterogeneous in the actin protomers. On the other hand, the formin binding evoked a decrease of the mobility in the saturation transfer EPR time domain, which is characteristic for the torsional motion of the filaments. Although the motions on these two substantially different timescales could be correlated, the correlation is probably complex. According to our results, the effects of formin on these two different types of motions were uncoupled and appeared to be independent of each other. In these cases, one can assume that the formin-induced changes are manifested by different molecular mechanisms. The elucidation of the details of these intraprotein mechanisms requires further investigations.

This study was supported by grants from the Hungarian Science Foundation (OTKA grant No. K60186 and K60968 (Miklós Nyitrai)), and from the Hungarian National Office for Research and Technology (grants GVOP-3.2.1.-2004-04-0190/3.0 and GVOP-3.2.1.-2004-04-0228/3.0). Miklós Nyitrai holds a Wellcome Trust International Senior Research Fellowship in Biomedical Sciences.

REFERENCES

1. Pantaloni, D., C. Le Clainche, and M. F. Carlier. 2001. Mechanism of actin-based motility. *Science*. 292:1502–1506.
2. Pollard, T. D., L. Blanchoin, and R. D. Mullins. 2000. Molecular mechanisms controlling actin filament dynamics in nonmuscle cells. *Annu. Rev. Biophys. Biomol. Struct.* 29:545–576.
3. Sheterline, P., J. Clayton, and S.J.C. 1998. Protein profiles. Actin. P. Sheterline, J. Clayton, and J.C. Sparrow, editors. New York: Oxford Univ. Press.
4. Egelman, E. H., N. Francis, and D. J. DeRosier. 1982. F-actin is a helix with a random variable twist. *Nature*. 298:131–135.
5. Egelman, E. H., and A. Orlova. 1995. New insights into actin filament dynamics. *Curr. Opin. Struct. Biol.* 5:172–180.
6. Orlova, A., and E. H. Egelman. 1993. A conformational change in the actin subunit can change the flexibility of the actin filament. *J. Mol. Biol.* 232:334–341.
7. Pollard, T. D., and G. G. Borisy. 2003. Cellular motility driven by assembly and disassembly of actin filaments. *Cell*. 112:453–465.
8. Allingham, J. S., V. A. Klenchin, and I. Rayment. 2006. Actin-targeting natural products: structures, properties and mechanisms of action. *Cell. Mol. Life Sci.* 63:2119–2134.
9. Dominguez, R. 2004. Actin-binding proteins–a unifying hypothesis. *Trends Biochem. Sci.* 29:572–578.
10. Orlova, A., and E. H. Egelman. 1995. Structural dynamics of F-actin: I. Changes in the C terminus. *J. Mol. Biol.* 245:582–597.
11. Bugyi, B., G. Papp, G. Hild, D. Lorinczy, E. M. Nevalainen, et al. 2006. Formins regulate actin filament flexibility through long range allosteric interactions. *J. Biol. Chem.* 281:10727–10736.
12. Shimada, A., M. Nyitrai, I. R. Vetter, D. Kuhlmann, B. Bugyi, et al. 2004. The core FH2 domain of diaphanous-related formins is an elongated actin binding protein that inhibits polymerization. *Mol. Cell.* 13:511–522.
13. Spudich, J. A., and S. Watt. 1971. The regulation of rabbit skeletal muscle contraction. I. Biochemical studies of the interaction of the tropomyosin-troponin complex with actin and the proteolytic fragments of myosin. *J. Biol. Chem.* 246:4866–4871.

14. Feuer, G., F. Molnár, E. Pettkó, and F. B. Straub. 1948. Studies on the composition and polymerisation of actin. *Hung. Acta. Physiol.* 1:150–163.

15. Squier, T. C., and D. D. Thomas. 1986. Methodology for increased precision in saturation transfer electron paramagnetic resonance studies of rotational dynamics. *Biophys. J.* 49:921–935.

16. Fajer, P. G., and D. Marsh. 1982. Microwave and modulation field inhomogneitis and the effect of cavity Q in saturation EPR spectra. Dependence of sample size. *J. Magn. Reson.* 49:212–224.

17. Budil, D. E., S. Lee, S. Saxena, and J. H. Freed. 1996. Nonlinear-least-squares analysis of slow-motion EPR spectra in one and two dimensions using modified Levenberg-Marquard algorithm. *J. Magn. Reson.* 120:155–189.

18. Meirovitch, E., A. Nayeem, and J. H. Freed. 1984. Analysis of protein-lipid interaction based on model simulation of electron spin resonance spectra. *J. Phys. Chem.* 88:3454–3465.

19. Szabó, Z., M. Budai, K. Blaskó, and P. Gróf. 2004. Molecular dynamics of the cyclic lipodepsipeptides' action on model membranes: effects of syringopeptin22A, syringomycin E, and syringotoxin studied by EPR technique. *Biochim. Biophys. Acta.* 1660:118–130.

20. Mossakowska, M., J. Belagyi, and H. Strzelecka-Golaszewska. 1988. An EPR study of the rotational dynamics of actins from striated and smooth muscle and their complexes with heavy meromyosin. *Eur. J. Biochem.* 175:557–564.

21. Thomas, D. D., J. C. Seidel, and J. Gergely. 1979. Rotational dynamics of spin-labeled F-actin in the sub-millisecond time range. *J. Mol. Biol.* 132:257–273.

22. Yoshimura, H., T. Nishio, K. Mihashi, K. Kinosita, Jr., and A. Ikegami. 1984. Torsional motion of eosin-labeled F-actin as detected in the time-resolved anisotropy decay of the probe in the sub-millisecond time range. *J. Mol. Biol.* 179:453–467.

23. Prochniewicz, E., Q. Zhang, E. C. Howard, and D. D. Thomas. 1996. Microsecond rotational dynamics of actin: spectroscopic detection and theoretical simulation. *J. Mol. Biol.* 255:446–457.

24. Lu, R. C., and L. Szilagyi. 1981. Change of reactivity of lysine residues upon actin polymerization. *Biochemistry.* 20:5914–5919.

25. Waring, A. J., and R. Cooke. 1987. The molecular dynamics of actin measured by a spin probe attached to lysine. *Arch. Biochem. Biophys.* 252:197–205.

26. Burtnick, L. D. 1984. Modification of actin with fluorescein isothiocyanate. *Biochim. Biophys. Acta.* 791:57–62.

27. Goldman, A. A., G. V. Bruno, and J. H. Freed. 1972. Estimating slow-motional rotational correlation times for nitroxides by electron spin resonance. *J. Phys. Chem.* 76:1858–1860.

28. Prochniewicz, E., and D. D. Thomas. 1997. Perturbations of functional interactions with myosin induce long-range allosteric and cooperative structural changes in actin. *Biochemistry.* 36:12845–12853.

29. Mason, R. P., and J. H. Freed. 1974. Estimating microsecond rotational correlation times from lifetime broadening of nitroxide electron spin resonance spectra near the rigid limit. *J. Phys. Chem.* 78:1321–1323.

30. Schreier, S., C. F. Polnaszek, and I. C. Smith. 1978. Spin labels in membranes. Problems in practice. *Biochim. Biophys. Acta.* 515: 395–436.

31. Thomas, D. D., L. R. Dalton, and J. S. Hyde. 1976. Rotational diffusion studied by passage saturation transfer electron paramagnetic resonance. *J. Chem. Phys.* 65:3006–3023.

32. Papp, G., B. Bugyi, Z. Ujfalusi, S. Barko, G. Hild, et al. 2006. Conformational changes in actin filaments induced by formin binding to the barbed end. *Biophys. J.* 91:2564–2572.

33. Li, F., and H. N. Higgs. 2003. The mouse formin mDia1 is a potent actin nucleation factor regulated by autoinhibition. *Curr. Biol.* 13:1335–1340.

34. Romero, S., C. Le Clainche, D. Didry, C. Egile, D. Pantaloni, et al. 2004. Formin is a processive motor that requires profilin to accelerate actin assembly and associated ATP hydrolysis. *Cell.* 119:419–429.

35. Lőrinczy, D., F. Könczöl, B. Gaszner, and J. Belágyi. 1998. Structutal stability of actin as studied by DSC and EPR. *Thermochim. Acta.* 322:95–100.

36. Kim, E., E. Bobkova, C. J. Miller, A. Orlova, G. Hegyi, et al. 1998. Intrastrand cross-linked actin between Gln-41 and Cys-374. III. Inhibition of motion and force generation with myosin. *Biochemistry.* 37:17801–17809.